Effect of the Orientation of the Ester Bonds on the Properties of Three Isomeric Liquid Crystal Diacrylates before and after Polymerization

R. A. M. Hikmet,* J. Lub, and A. J. W. Tol

Philips Research, WB72, Prof. Holstlaan 4, 5656AA Eindhoven, The Netherlands

Received December 8, 1994; Revised Manuscript Received February 8, 1995[⊗]

ABSTRACT: Three isomeric liquid crystal (LC) acrylates 1,4-bis((4-((6-(acryloyloxy)hexyl)oxy)benzoyl)-oxy)benzene, ((6-(acryloyloxy)hexyl)oxy)-4-((4-((4-((6-(acryloyloxy)hexyl)oxy)benzoyl)oxy)benzoyl)oxy)-benzene, and bis(4-((6-(acryloyloxy)hexyl)oxy)phenyl) terephthalate were synthesized. The orientation of the ester links with respect to the central phenyl ring has a strong influence on the phase, optical, and dielectric behavior of the monomers. The polymerization behavior of the isomers was found to differ. Changes occurring in the microstructure during polymerization were studied using X-ray diffraction. In order to obtain an understanding of the observed differences, the phase behavior and polymerization behavior of various mixtures were studied. The results of the experiments and the molecular modeling suggested that the associations between the molecules is the origin of the formation of observed LC phases and the strength of the interactions determine whether the microstructure is preserved during polymerization.

1. Introduction

In-situ photopolymerization of liquid crystal molecules can be used in the production of anisotropic networks, gels and plasticized networks[1−9]. The technique of in-situ photopolymerization involves the macroscopic orientation of liquid crystal molecules with reactive end groups followed by UV radiation. In this way the molecular orientation within the system becomes fixed by the creation of a three-dimensional anisotropic network. In our previous publications polymerizations in the nematic,[1−4] smectic A,[5]cholesteric,[6,7] blue,[8] and ferroelectric[9] phases have been described. It was shown that upon polymerization macroscopic properties such as a high birefringence in the nematic phase, optical activity (selective reflection of circularly polarized light) in the cholesteric phase, and macroscopic dipolar orientation, and hence piezoelectricity, in the ferroelectric phase were preserved during polymerization. In these publications bifunctional molecules used in cross-linking had the same central structure as monomer **1** shown in Figure 1. In the present publication we describe the synthesis of two other isomers of this molecule. The orientations of the ester bonds in these isomers were changed. Several properties of the isomers in the monomeric state have been examined, and the effect of the molecular structure on the polymerization behavior has been studied. Association between the molecules and the steric hindrance on sustaining the macroscopic as well as the microscopic structure upon polymerization will be discussed. Theoretical calculations have been performed to obtain an understanding of the conformational and electrostatic nature of the molecules in order to be able to explain the observed behavior.

2. Experimental Section

2.1. Monomer Synthesis. The structures of the monomers are shown in Figure 1. All the solvents were obtained from Merck. All other chemicals were obtained from Janssen Chimica, except for thionyl chloride, which was obtained from Merck. The syntheses of bis((4-((6-(acryloyloxy)hexyl)oxy)benzoyl)oxy)benzene (**1**) and of 4-((6-(acryloyloxy)hexyl)oxy)benzoic acid (**11**) have been described previously.[10] All diacrylates were more than 97% pure according to HPLC. All the products exhibit ^{1}H-NMR spectra (300 MHz) that are in accordance with their structures.

2.1.1. Synthesis of ((6-(Acryloyloxy)hexyl)oxy)-4-((4-((4-((6-(acryloyloxy)hexyl)oxy)benzoyl)oxy)-benzoyl)oxy)benzene (2) (Scheme 1) and of Bis(4-((6-(acryloyloxy)hexyl)oxy)phenyl) Terephthalate (3) (Scheme 2). 4-(Tetrahydropyran-2-yloxy)phenol. (4). To a mixture of 110 g of hydroquinone (1.0 mol), 8.5 g of 4-toluenesulfonic acid (0.05 mol), and 1 L of diethyl ether was added 90 mL of dihydropyran (1.0 mol) over a period of 30 min with stirring. After stirring for two more hours, the solution was filtered and nitrogen was bubbled through. The solution was extracted twice with nitrogen-purged solutions of 22.5 g of sodium hydroxide in 300 mL of water (total: 1.12 mol). The combined aqueous solutions were extracted with 250 mL of diethyl ether and were cooled to 0 °C with ice. Sodium bicarbonate (5 g) was added, and the vigorously stirred solution was slowly acidified with 64 mL of acetic acid (1.12 mol). The precipitated crude product was washed twice with 300 mL of water and dried over silica under a vacuum. The yield was 78 g (40%).

4-(Tetrahydropyran-2-yloxy)((6-hydroxyhexyl)-oxy)benzene (5). To a nitrogen-purged solution of 78 g of 4-(tetrahydropyran-2-yloxy)phenol (**4**) (0.4 mol) in 250 mL of butanone was added 22 g of sodium methanolate (0.4 mol). After a clear solution was obtained 12 g of sodium iodide (0.08 mol) and 46 mL of 6-chlorohexanol (0.4 mol) were added. After the solution was boiled for 24 h, it was filtered and evaporated. To the remaining oil were added 250 mL of diethyl ether and 100 mL of water. After separation, the ether layer was extracted twice using 50 mL of a 10% sodium hydroxide solution and once using 50 mL of a saturated sodium chloride solution and was then dried over magnesium sulfate. The crude product obtained after evaporation

[⊗] Abstract published in *Advance ACS Abstracts,* March 15, 1995.

0024-9297/95/2228-3313$09.00/0

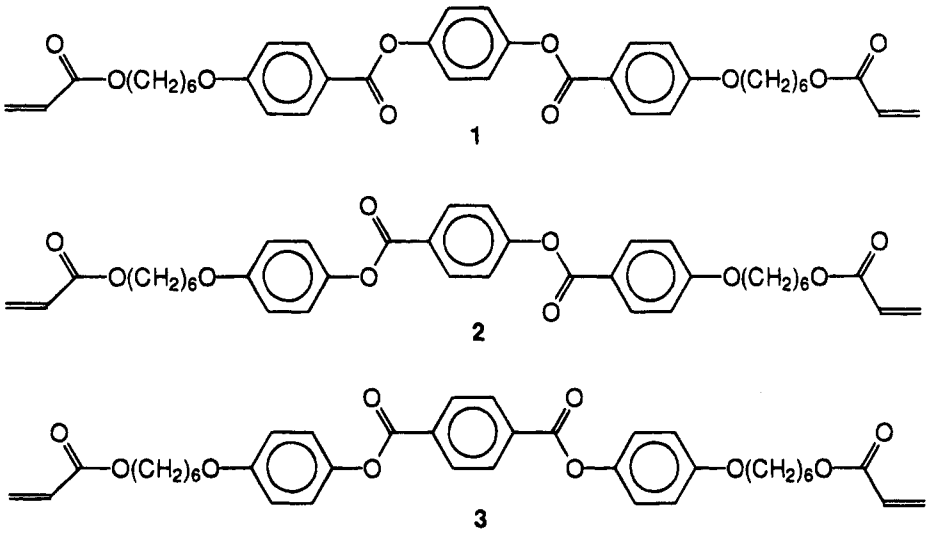

Figure 1. Structure of the isomers.

of the diethyl ether was washed for 30 min with 250 mL of pentane to remove unreacted 6-chlorohexanol. The product obtained after drying over silica under a vacuum was a white powder. Yield: 94 g (80%).

4-((6-(Acryloyloxy)hexyl)oxy)phenol. (7). To a solution of 94 g of 4-(tetrahydropyran-2-yloxy)((6-hydroxyhexyl)oxy)benzene (**5**) (0.32 mol), 68 mL of triethylamine (0.48 mol), and 0.1 g of 6-di-*tert*-butyl-4-methylphenol in 400 mL of dichloromethane was added 31 mL of acryloyl chloride (0.38 mol) over a period of 30 min. After the mixture had been stirred for 16 h, 250 mL of an ice-cold 1 N hydrochloric acid solution was added. After separation and evaporation of the dichloromethane, 4-(tetrahydropyran-2-yloxy)((6-(acryloyloxy)hexyl)oxy)benzene (**6**) was obtained. This was added to a mixture of 500 mL of ethanol and 10 g of pyridinium 4-toluenesulfonate (0.04 mol). After this mixture had been heated to 60 °C and maintained at this temperature for 2 h, it was poured into a vigorously stirred mixture of 600 mL of water and 300 g of ice. The precipitated product was washed with 200 mL of water and dried over silica under a vacuum. Yield: 63.3 g (75%) of a light yellow powder.

4-(Tetrahydropyran-2-yloxy)benzoic Acid. (8). To a mixture of 138 g of 4-hydroxybenzoic acid (1.0 mol), 8.5 g of 4-toluenesulfonic acid (0.05 mol), and 1 L of diethyl ether was added 135 mL of dihydropyran (1.5 mol) over a period of 30 min with stirring. After the stirring had been continued for 16 h, the precipitate was filtered off. It was washed with 600 mL of diethyl ether and dried over silica under a vacuum. The yield was 111 g (52%) of a white powder.

((6-(Acryloyloxy)hexyl)oxy)-4-((4-hydroxybenzoyl)oxy)benzene (10). To a mixture of 26.4 g of 4-((6-(acryloyloxy)hexyl)oxy)phenol (**7**), 11.1 g of 4-(tetrahydropyran-2-yloxy)benzoic acid (**8**), 1.5 g of *N,N*-(dimethylamino)pyridine in 200 mL of dichloromethane, cooled to 0 °C, was added 22 g of *N,N'*-dicyclohexylcarbodiimide. After this mixture had been stirred for 24 h at room temperature, it was filtered and evaporated. Crude ((6-(acryloyloxy)hexyl)oxy)-4-((4-(tetrahydropyran-2-yloxy)benzoyl)oxy)benzene (**9**) was crystallized from ethanol. This was added to a mixture of 250 mL of ethanol and 5 g of pyridinium 4-toluenesulfonate (0.02 mol). After this mixture had been heated to 60 °C and maintained at this temperature for 4 h, it was poured into a vigorously stirred mixture of 400 mL of water and 200 g of ice. The precipitated product was washed with 200 mL of water and dried over silica under a vacuum. Yield: 30.0 g (78%) of a white powder.

((6-(Acryloyloxy)hexyl)oxy)-4-((4-((4-((6-(acryloyloxy)hexyl)oxy)benzoyl)oxy)benzoyl)oxy)benzene (2). To a mixture of 14.2 g of 4-((6-(acryloyloxy)-hexyl)oxy)benzoic acid (**11**) (0.05 mol), 0.4 mL of dimethylformamide, 0.2 g of 2,6-di-*tert*-butyl-4-methylphenol, and 100 mL of CH_2Cl_2, through which a stream of dry nitrogen was bubbled, was added 6 mL of thionyl chloride (0.08 mol). After overnight stirring, the dichloromethane and thionyl chloride were evaporated, first at 40 °C and then at room temperature and under high vacuum. To this acid chloride were added 100 mL of dichloromethane and 11 mL of triethylamine (0.08 mol). After cooling in an ice bath, 19.2 g of ((6-(acryloyloxy)-hexyl)oxy)-4-((4-(hydroxybenzoyl)oxy)benzene (10) (0.05 mol) was added in portions at such a rate that the reaction temperature did not exceed 20 °C. After stirring for 3 days at room temperature a mixture of 50 g of ice, 50 mL of water, and 2 mL of concentrated hydrochloric acid solution was added. After separation, the organic layer was extracted with 80 mL of a concentrated sodium chloride solution. The organic layer was then eluted over magnesium sulfate (column diameter 40 mm, column height 10 mm) and over silica (same dimensions). A colorless solution was obtained which was evaporated at 30 °C to yield the crude product as a white waxy solid. This solid was crystallized twice with filtration the first time, from 2-propanol to which small amounts of 4-methoxyphenol were added. After drying over silica under vacuum, 22.7 g of the product (69%) was obtained as white plates.

2.1.2. Synthesis of Bis(4-((6-(acryloyloxy)hexyl)-oxy)phenyl) Terephthalate (3). To a cooled solution of 26.4 g of 4-((6-(acryloyloxy)hexyl)oxy)phenol (**7**) (0.10 mol), 21 mL of triethylamine (0.15 mol), and 0.2 g of 2,6-di-*tert*-butyl-4-methylphenol in 150 mL of dichloromethane was added 10.2 g of terephthaloyl chloride (0.05 mol) in portions at such a rate that the reaction temperature did not exceed 20 °C. After stirring for 3 days at room temperature, a mixture of 50 g of ice, 50 mL of water, and 2 mL of concentrated hydrochloric acid solution was added. The organic layer after separation was extracted using 80 mL of a concentrated sodium chloride solution. The organic layer was then eluted over magnesium sulfate (column diameter 40 mm, column height 10 mm) and over silica (same dimensions). A colorless solution was obtained, which was

Scheme 1. Synthetic Route to ((6-(Acryloyloxy)hexyl)oxy)-4-((4-((4-((6-(acryloyloxy)hexyl)oxy)benzoyl)oxy)benzoyl)oxy)benzene (2)

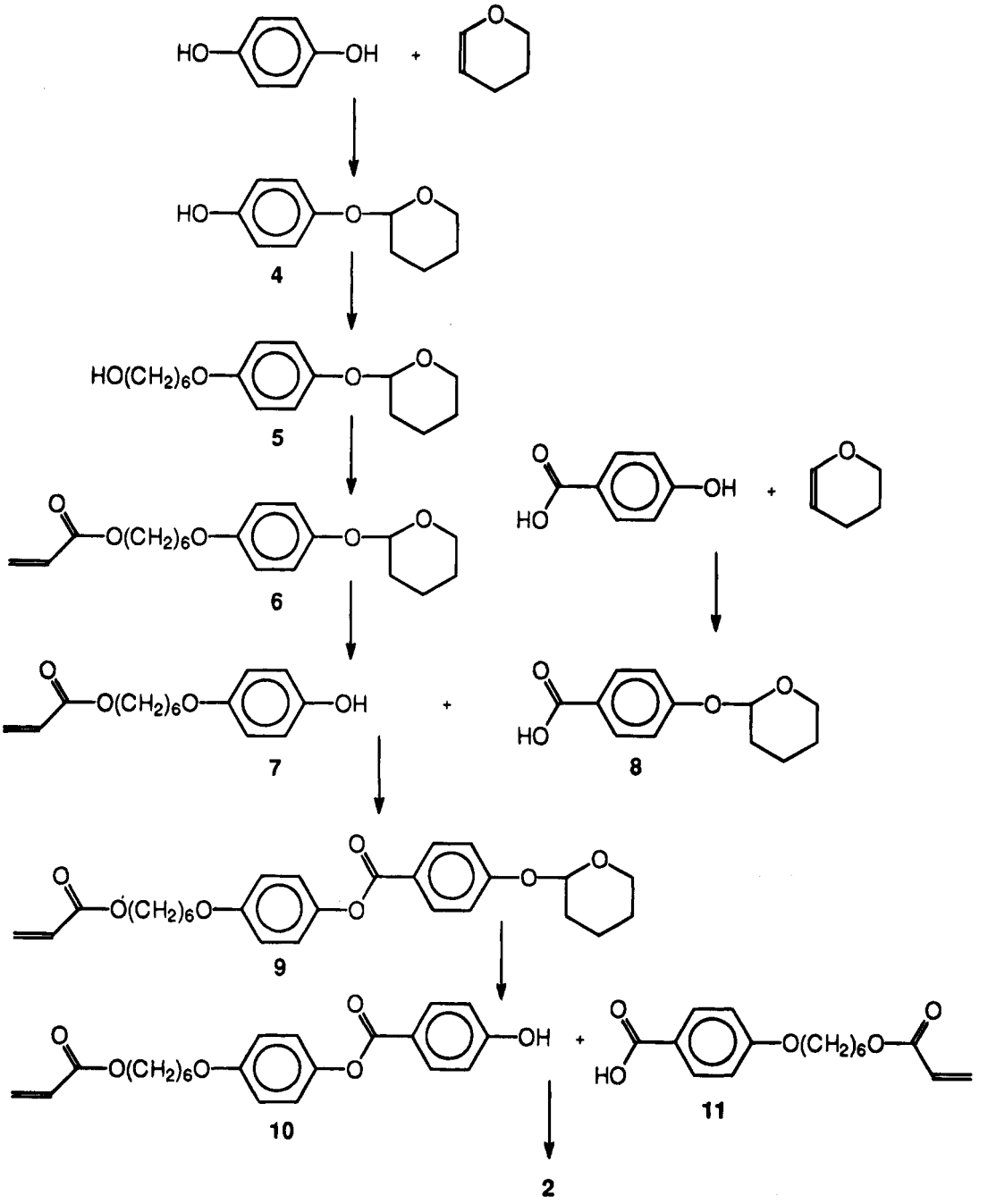

Scheme 2. Synthetic Route to Bis(4-((6-(acryloyloxy)hexyl)oxy)phenyl) Terephthalate (3)

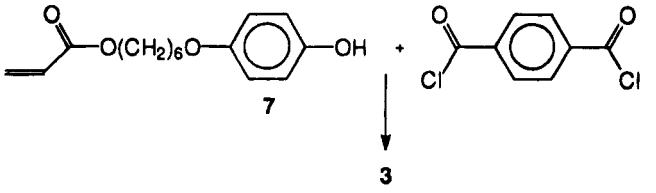

evaporated at 30 °C to yield the crude product, which was crystallized twice, the first time with filtration, from 2-propanol to which small amounts of 4-methoxyphenol were added. After drying over silica under a vacuum, 15.0 g of the product (45%) was obtained in the form of needles.

2.2. Methods. The refractive indices of the molecules were measured using an Abbe refractometer which could be thermostated up to 140 °C. Uniaxial orientation of the molecules was induced in glass cells provided with uniaxially rubbed nylon layers. The birefringence measurements were carried out using a polarizing microscope equipped with a compensator and a Mettler FP82 hot stage. For the transmission/voltage measurements the microscope was provided with a photomultiplier. The transition temperatures and enthalpies were measured using a Perkin Elmer DSC7. The dielectric measurements were carried out using a Hewlett-Packard Impedance/Phase Gain analyzer. The X-ray diffraction measurements were carried out using a Statton camera and Ni-filtered Cu Kα radiation from a Philips X-ray generator.

3. Results and Discussion

3.1. Monomers. The synthetic routes to monomers **2** and **3** are presented in Schemes 1 and 2, respectively.

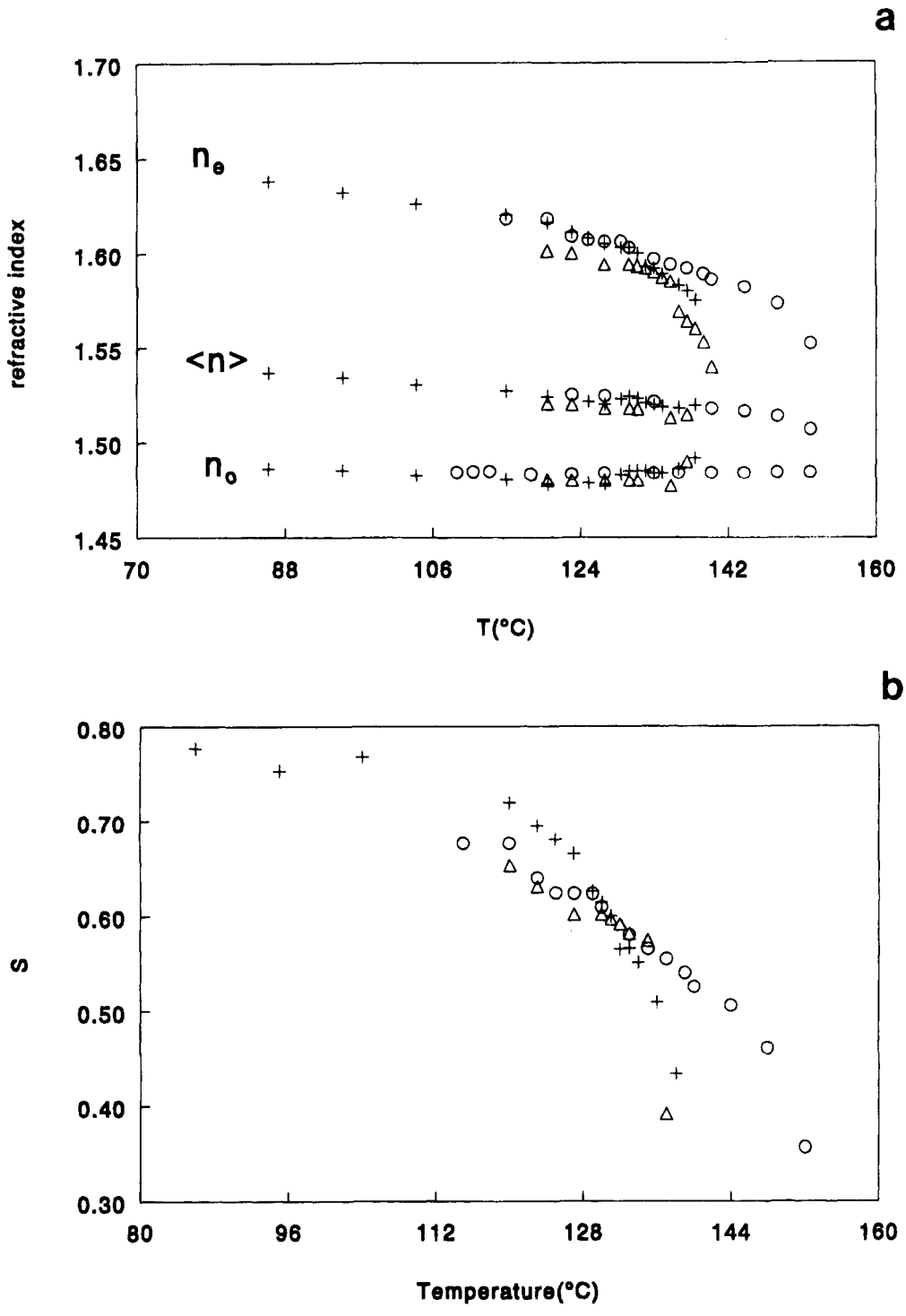

Figure 2. (a) Refractive indices and (b) order parameters of various monomers: ○ = **1**, + = **2**, △ = **3**.

Both compounds contain the hydroquinone moiety in an asymmetrically substituted form. In order to avoid complicated purification procedures, one of the hydroxyl groups of the hydroquinone was protected as a tetrahydropyranyl ether (see scheme 2). This protected species is relatively easy to make,[11,12] while deprotection occurs smoothly without having an effect on the newly formed ether and ester bonds in intermediate **6**. The same holds for the deprotection of intermediate **9**, in which the hydroxybenzoate moiety is introduced with the aid of the protected hydroxybenzoic acid **8**. Intermediate **7**, which was prepared so as to be able to produce monomer **2**, can also be used to form monomer **3** (see Scheme 2).

The transition temperatures of the three isomeric monomers are shown below:

1	S_c	(81 °C)	K	108 °C	N	152 °C	I
2	K	73 °C	S_a	132 °C	N	145 °C	I
3	K	116 °C	S_a	135 °C	N	140 °C	I

It can be seen that molecules **2** and **3** show smectic-A (S_a) phases whereas isomer **1** shows a monotropic smectic-C (S_c) phase. The phase behavior observed here is very similar to that of the molecules of this type without reactive end groups.[13] The refractive indices of the monomers are shown in Figure 2a. For monomer **1** the ordinary refractive index (n_o) above 140 °C was assumed to be constant and the extraordinary refractive

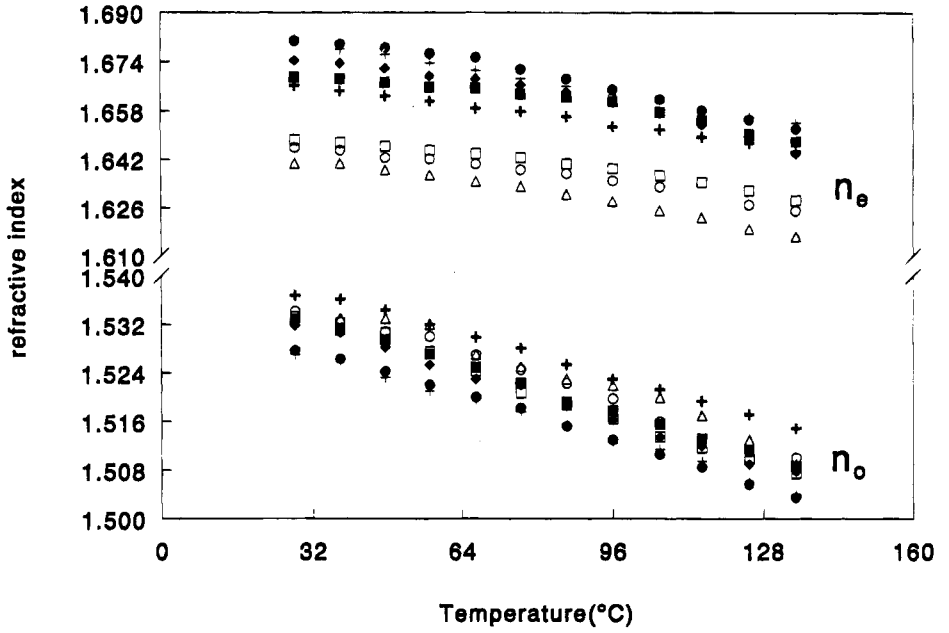

Figure 3. Refractive indices of the networks produced by polymerization at various temperatures: crosses = **1**, closed symbols = **2**, open symbols = **3**; ● = 100, ♦ = 130, ■ = 135, + = 85, + = 148, △ = 80, ○ = 112 , □ = 138 °C.

index (n_e) was estimated from birefringence measurements. The mean refractive index $\langle n \rangle$ of the samples was calculated using the equation $\langle n \rangle = (2n_o + n_e)/3$. In Figure 2a it can be seen that in all cases n_o remains almost constant whereas n_e decreases with increasing temperature. If the birefringence values of the samples measured at temperatures sufficiently far from their isotropic transition temperatures are compared, it can be seen that monomers **1** and **2** have very similar values while monomer **3** shows a lower birefringence. In Figure 2 another difference between monomer **3** and its isomers can be observed concerning their $\langle n \rangle$. At a given temperature the $\langle n \rangle$ values of monomers **1** and **2** are about the same, that of monomer **3** is lower. As the building blocks of the molecules are the same, it can be concluded that the difference in $\langle n \rangle$ is caused by the difference in the densities. The difference in Δn may be a result of the difference in the order parameter. These points will be further dealt with in the discussion of the theoretically calculated conformation and related properties of the molecules. We estimated the order parameter S for the monomers on the basis of the refractive indices using the equation below

$$S = C\frac{3(n_e^2 - n_o^2)}{n_e^2 + 2n_o^2 - 3} \tag{1}$$

where $C = (\alpha/\alpha_{\parallel} - \alpha_{\perp})$ and $\alpha_{\parallel}$, $\alpha_{\perp}$ are the molecular polarizabilities in the directions parallel and perpendicular to the molecular orientation, respectively, and the mean polarizability is given by α. The constant C

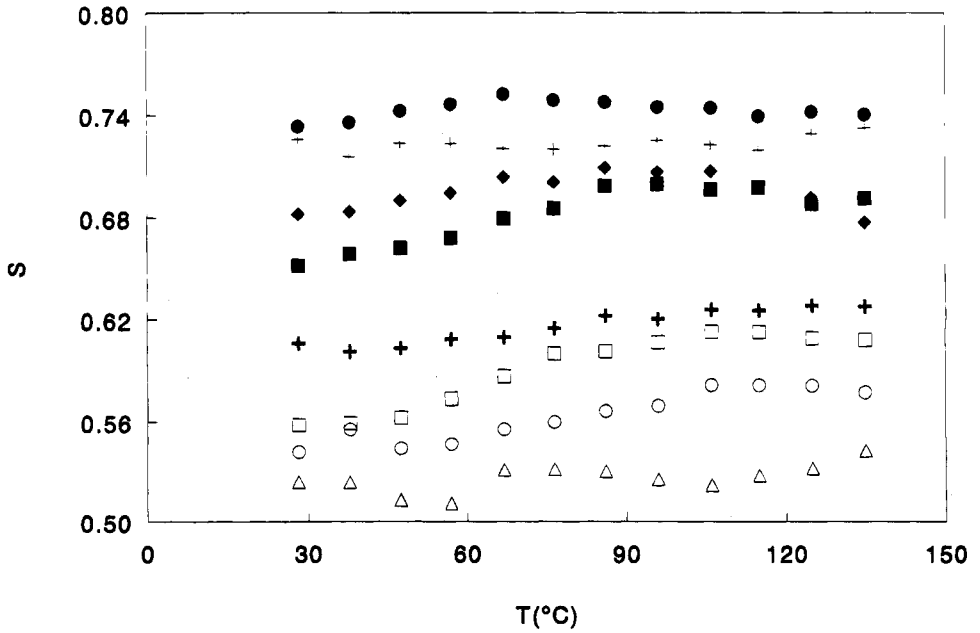

Figure 4. Order parameter as a function of temperature for various networks: crosses = **1**, closed symbols = **2**, open symbols = **3**; ● = 100, ♦ = 130, ■ = 135, + = 85, + = 148, △ = 80, ○ = 112, □ = 138 °C.

was calculated for molecules **1**–**3** using molecular modeling (see the section on modeling) and was found to be 2.192, 2.236, and 2.243, respectively. The value C calculated for molecule **1** using molecular modeling agrees well with the value experimentally obtained in our previous work.[3] By inserting the constants C and the refractive indices in the equation above, we estimated the order parameters of the monomers; the results are shown in Figure 2b. It can be seen that the order parameters of the molecules are very similar, at low temperatures, whereas they diverge at higher temperatures, especially at temperatures close to their clearing temperatures.

3.2. Polymerization of the Monomers. Macroscopic orientation of the monomers was induced on rubbed nylon. Polymerization was initiated using a UV source. In the case of monomers **1** and **2** the samples were still transparent after polymerization, whereas in the case of monomer **3**, samples changed their appearances depending on the temperature of polymerization. Especially those polymerized in the S_a phase showed diffraction colors when held against a light source. In order to be able to characterize the polymerized samples, we measured their optical anisotropy at various temperatures. In Figure 3 the refractive indices of various anisotropic networks produced by polymerization at various temperatures are plotted as a function of the temperature. It can be seen that in the case of monomers **1** and **2** the birefringence of the anisotropic networks increases, with decreasing polymerization temperature at a given temperature, whereas the opposite behavior is observed in the case of polymer **3**. It is important to mention that the refractive indices of the polymers of **1** and **2** could easily be measured using the refractometer whereas those of the polymers of **3**, especially those polymerized in the S_a phase, were difficult to measure. The behavior observed here can be associated with the order parameter within the system. We estimated the order parameter S for anisotropic networks from the refractive indices using eq 1. The same constants C calculated for the monomers were used in the calculations. This method has been shown to give good estimations of the order parameters.[2] The order parameter is plotted as a function of the temperature in Figure 4 where various effects can be seen. First the order parameter is in most cases not constant; for a given network it increases with temperature before showing a slight decrease at high temperatures. This indicates that the order in the networks formed at high temperatures decreases when they are cooled to room temperature. This decrease in the order parameter can be due to the density decrease and to steric interactions which make it difficult for the molecules to retain a good packing upon cooling. When the system is heated back to the polymerization temperature, the order increases reversibly. However, when the system is heated further above the polymerization temperature, thermal motion causes the order of the molecules to decrease.

The other effects that can be seen in Figure 4 are that the order parameter of molecules **1** and **2** increases with decreasing polymerization temperature and that at low polymerization temperatures (**1** at 85 °C and **2** at 100 °C) both polymers show almost the same order parameter. Monomer **3** showed the opposite behavior: the order parameter also decreased with a decreasing polymerization temperature. It is also interesting to compare the refractive indices (n_{iso}) of the polymers obtained by polymerization in the isotropic state. The n_{iso} values of **1**–**3**, were measured to be 1.583, 1.582, and 1.576, respectively. As the building blocks of all of the isomers are the same, the refractive indices of the molecules of the polymers would be expected to be the same (see molecular modeling). The fact that the n_{iso} values of molecule **3** differ significantly from those of isomers **1** and **2** indicates that the molecular packing and the density of isomer **3** also differ significantly from the packing and the density of isomers **1** and **2** in the isotropic state. X-ray diffraction measurements were carried out in order to study the changes taking place on the microscopic scale, after polymerization.

3.3. X-ray Diffraction. X-ray diffraction was used to characterize the changes in the molecular arrangement before and after polymerization. In Figure 5 we define the angles used further in the text in the description of the X-ray diffraction pattern (reciprocal space) and the corresponding molecular arrangements. The wide angle peaks (**W**) are caused by the rodlike molecules; they define the direction of molecular orientation. The small angle peaks (**S**) are due to the arrangement of the molecules with respect to one another.[14] In Figure 5a the X ray diffraction patterns of the molecules obtained in various smectic phases are shown. Monomers **2** and **3** exhibit typical S_a diffraction patterns showing broad equatorial wide angle peaks and sharper meridional ($\alpha = 90°$) small angle diffraction spots. In the case of isomer **1** the small angle peaks are off-meridional with $\alpha = 61°$. This is a characteristic of the S_c phase, where the smectic layers are tilted with respect to the director. In the present case the director is at an angle of 29° with respect to the smectic layer normal. The X-ray diffraction patterns of the molecules obtained in the nematic phase are shown in Figure 5b. In the nematic phase the small angle peaks become broader. This is mainly caused by the correlation lengths of the layers becoming shorter. In the case of molecule **1** the tilted orientation of the smectic layers remains present even in the nematic phase. This tilted orientation of the layers can most clearly be seen in the X-ray photo obtained at 92 °C where a four point pattern is apparent. In order to investigate this effect further, X-ray diffraction patterns were obtained at various temperatures in the nematic state (Figure 5). It can be seen that the four-point small angle patterns obtained at 92 °C become increasingly diffuse and eventually join up and take the form of meridional streaks. However, the fact that this tilted structure remains up to the high-temperature phase indicates that the driving force for this tilted arrangement of the molecules remains well in the nematic phase. Furthermore, the fact that α is almost temperature-independent suggests that this tilted orientation might be due to special interactions between the molecules.

The X-ray diffraction photos of the uniaxially oriented samples were also obtained after polymerization. In the case of molecules **1** and **2** the X-ray diffraction patterns were slightly sharper after polymerization and showed only a slight change in their position. The sharpening of the peaks is associated with the reduced thermal motion of the LC molecules as a result of polymerization. In the case of molecule **3**, however, changes were observed in the diffraction patterns. These changes were studied in two configurations: in homogeneously and homeotropically aligned samples. The diffraction photos shown in Figure 6a) were obtained for molecule

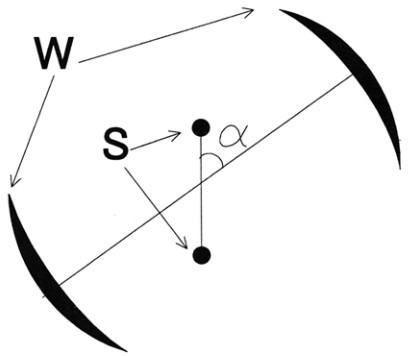

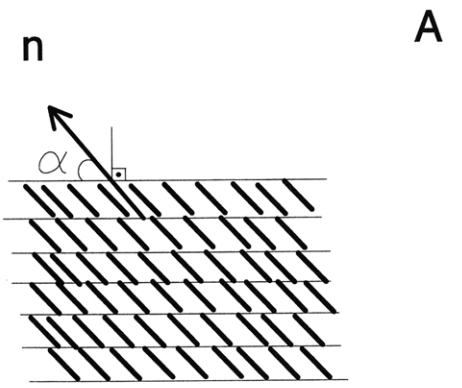

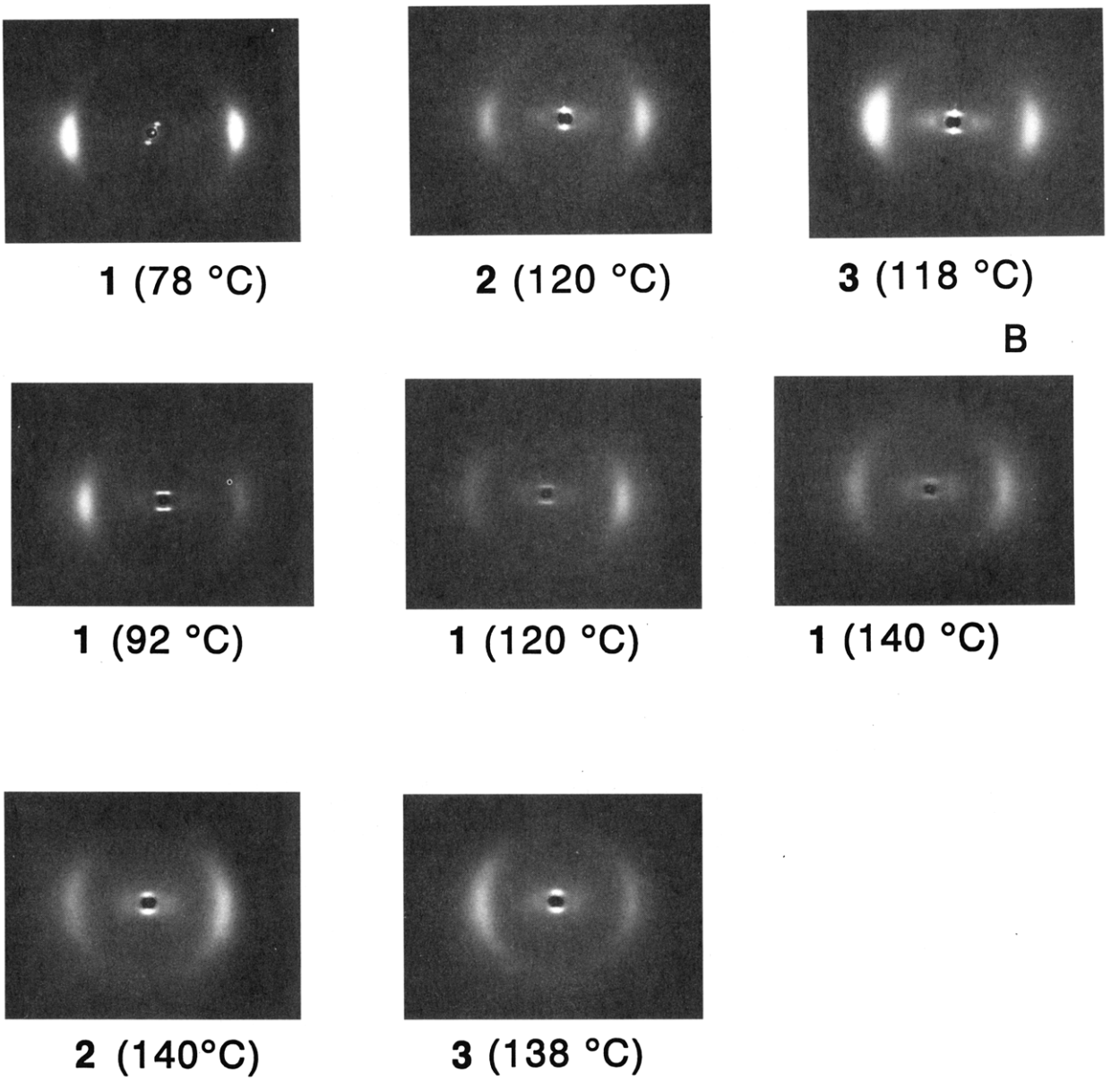

Figure 5. Schematic drawing of the X-ray diffraction pattern and corresponding molecular arrangement. X-ray diffraction patterns from various samples. (a) Smectic; (b) nematic phase.

3 polymerized in the S_a phase by placing the samples edge-on and flat-on to the horizontal X-ray beam so that the beam was perpendicular to the direction of molecular orientation. It can be seen that in the case of the homeotropically aligned samples the meridional small angle peaks split into three whereas in the case of the homogeneously oriented sample the peaks split into two. In both cases the equatorial wide angle peaks become broader. This effect was most clear in the case of the samples polymerized in the S_a phase. Those polymer-

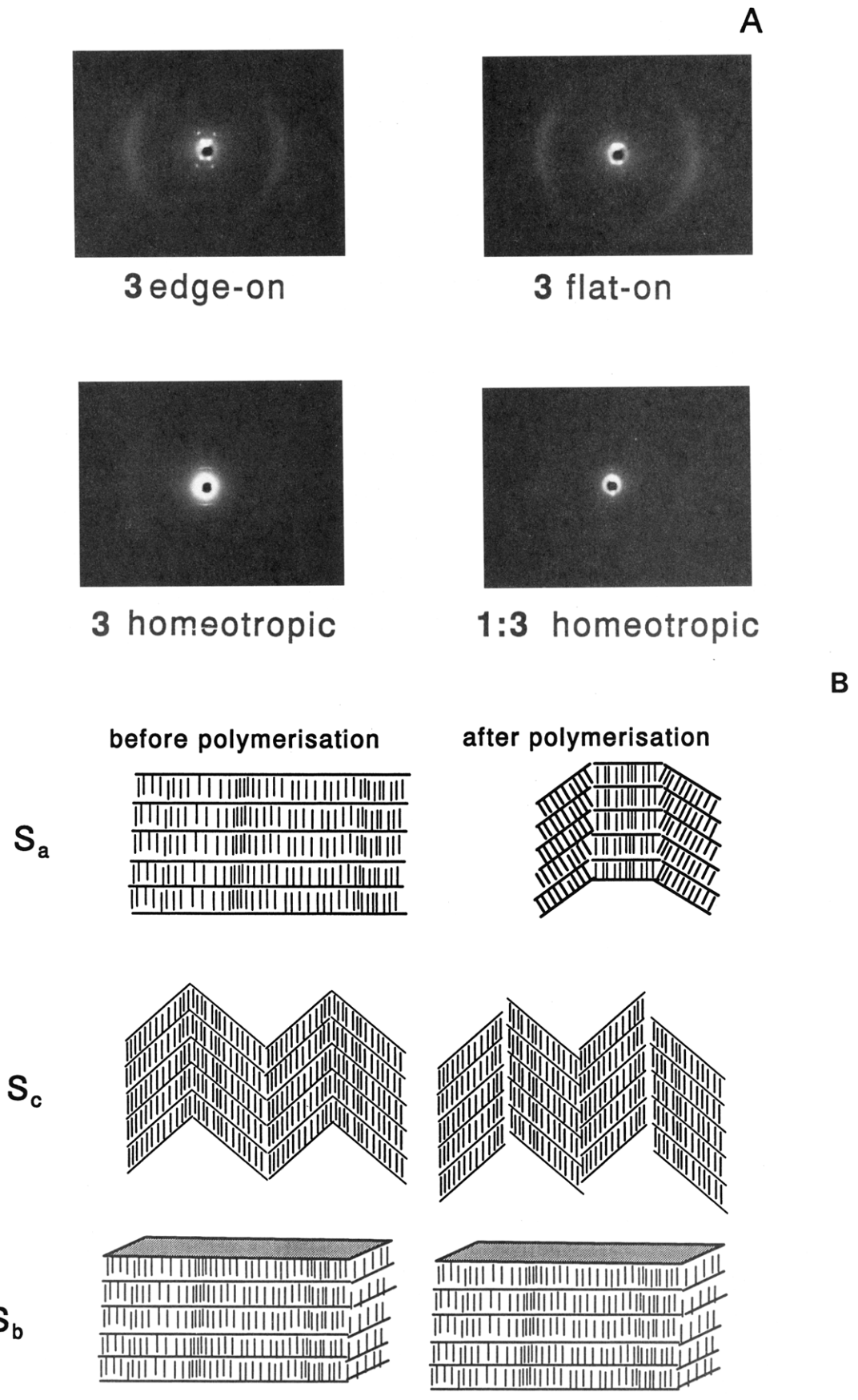

Figure 6. (a) X-ray diffraction patterns of **3** polymerized at 112 °C and **3** in a mixture with **1** (1:1) polymerized at 70 °C. (b) Schematic drawing of the changes as a result of polymerization of **3** (and its mixtures with **1**) in various smectic phases.

ized in the nematic phase, especially those polymerized at high temperatures, did not show the splitting of the meridional peaks too clearly. This is probably due to the nature of the layers in the different phases. In the S_a phase the correlation lengths are large. When the smectic layers break up and become disoriented, it can be detected by X-ray diffraction with ease. In the case of the nematic phase, the smectic like fluctuations occur

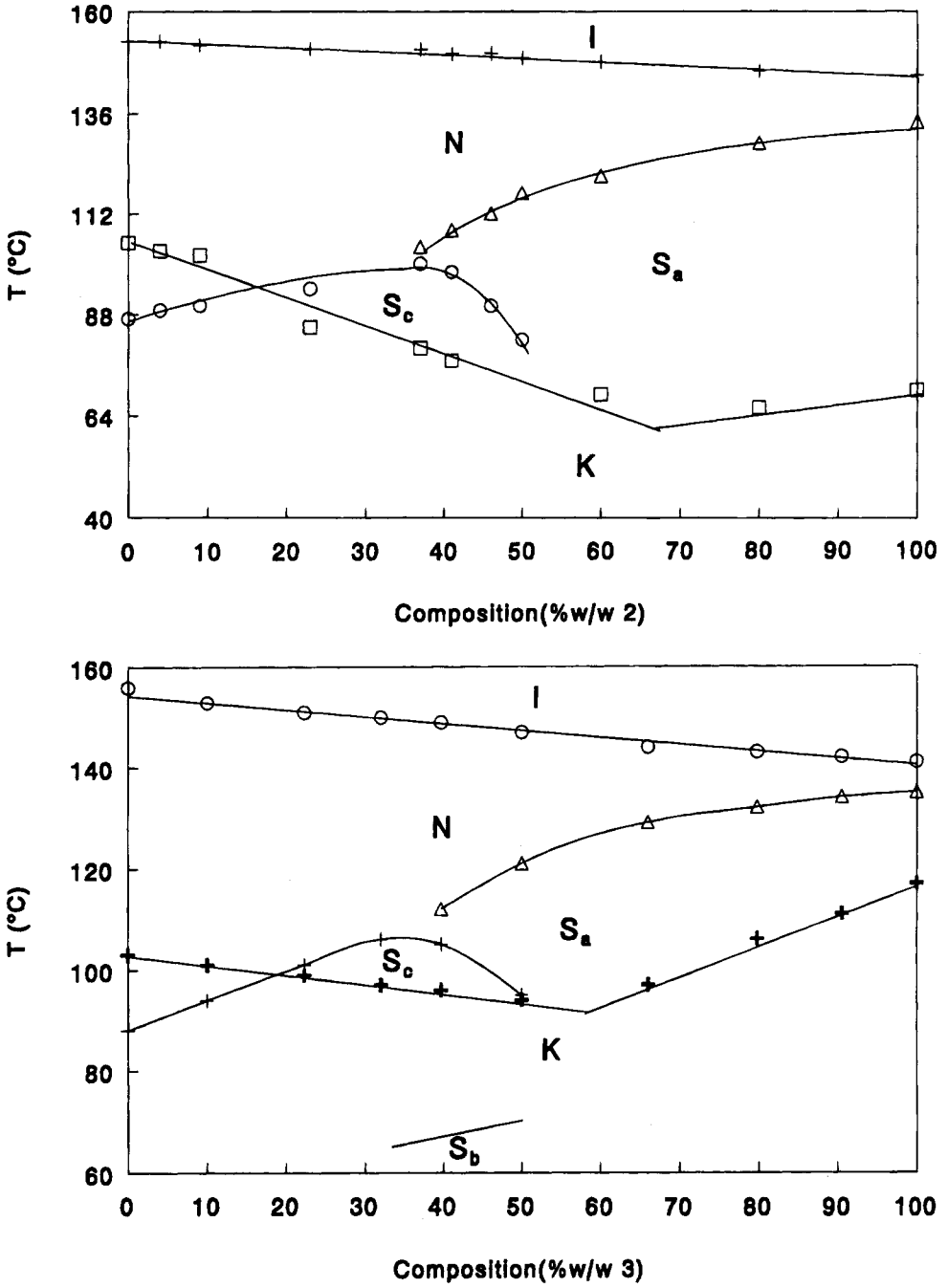

Figure 7. Binary phase diagrams of various mixtures with molecule **1**.

Table 1. Transition Enthalpies of Various Transitions in Various Compositions of the Binary Mixtures of 2 in 1

2 in 1%	ΔH(N→S_c) J/g	ΔH(N→S_a) J/g	ΔH(N→I), J/g
0	3.0		1.34
4	0.78		1.06
9	0.74		0.95
23	0.36		1.06
41		0.11	1.17
60		0.44	1.23
79		0.97	1.25
100		1.78	1.33

Table 2. Transition Enthalpies of Various Transitions in Various Compositions of the Binary Mixtures of 3 in 1

3 in 1%	ΔH(N→S_c) J/g	ΔH(N→S_a) J/g	ΔH(N→I) J/g
0	3.03		1.34
10	0.45		1.06
32			1.07
50		0.32	1.13
67		0.79	1.05
100		1.72	1.00

but the layers are already small. Any disorientation does therefore not show up very clearly. The broadening of the wide angle peaks is a result of the order parameter within the system. This was also observed in Figure 4. The changes in the microscopic structure of isomer **3** as a result of polymerization in the S_a phase deduced from the X-ray data are schematically shown in Figure 6b. It shows that after polymerization the smectic layers break up and some segments become tilted with respect to the initial direction of molecular orientation. This remarkably different behavior of isomer **3** may be due to various reasons: (i) the molecules have the tendency to form a tilted phase such as S_c; (ii) the association between the molecules is not strong enough to preserve the structure. In order to

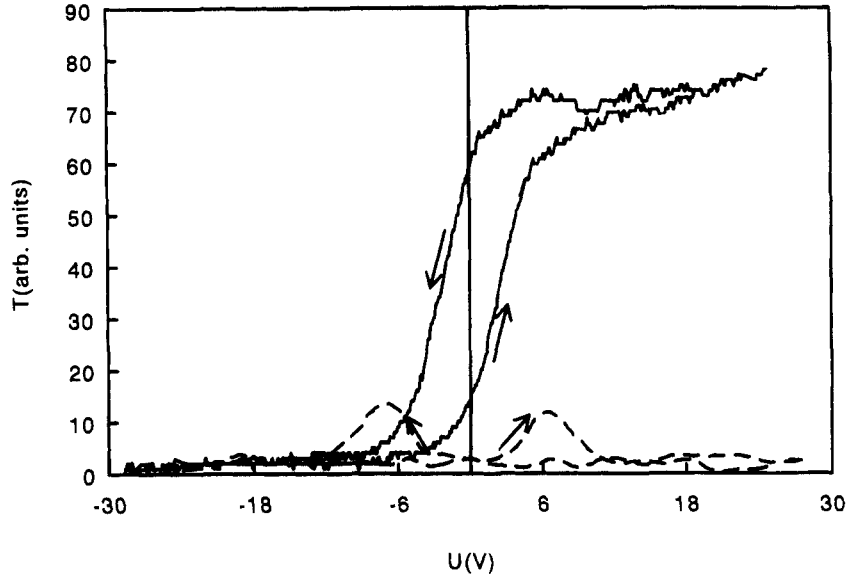

Figure 8. Transmission voltage behavior of pure **1** (broken line) and 66% w/w **1** with **3** (solid line).

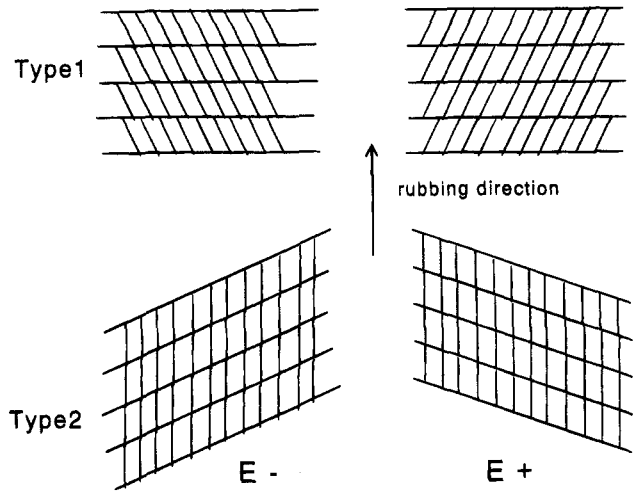

Figure 9. Schematic representation of various switchings.

investigate these effects we studied the isomers as binary mixtures.

3.4. Binary Mixtures. The phase behavior of the mixtures of monomers **3** and **1** was compared with that of monomers **2** and **1**. The results are shown in Figure 7. Both phase diagrams show that mixtures containing more than 50% w/w of monomer **1** show the S_c phase in addition to the S_a phase. Above 65% w/w of monomer **1** the S_a phase disappears and the mixtures only show the S_c phase. In all cases the nematic phase appears below the clearing point. In Tables 1 and 2 the enthalpies associated with various transitions are plotted for the binary mixtures of molecules **1** and **2** and **1** and **3**. In both cases the transition enthalpy from the nematic to the S_a phase increases with an increasing concentration of monomer **2** or **3**. At lower concentrations of monomer **2** or **3** the S_a phase disappears and in both systems the transition enthalpy from nematic to S_c increases with a decreasing concentration of monomer **2** or **3**. This indicates that the smectic transitions observed in the single components becomes weaker in both mixtures in about the same way. We further investigated the polymerization behavior of various binary mixtures using X-ray diffraction. After polymerization of the binary mixture of **1** and **2**, the microscopic structure is frozen-in the whole composition range at all temperatures. In the case of mixtures **1** and **3** a

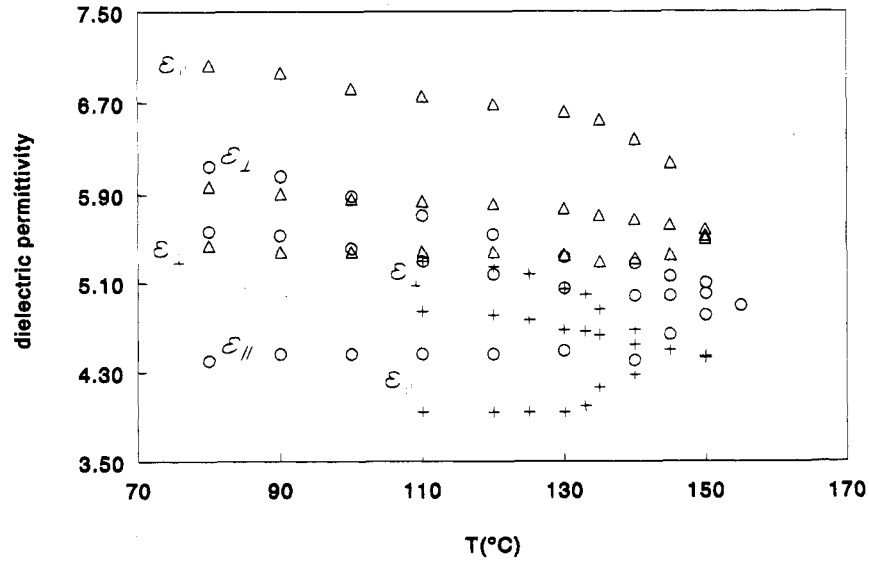

Figure 10. Dielectric permittivity of the monomers: ○ = **1**, △ = **2**, + = **3**.

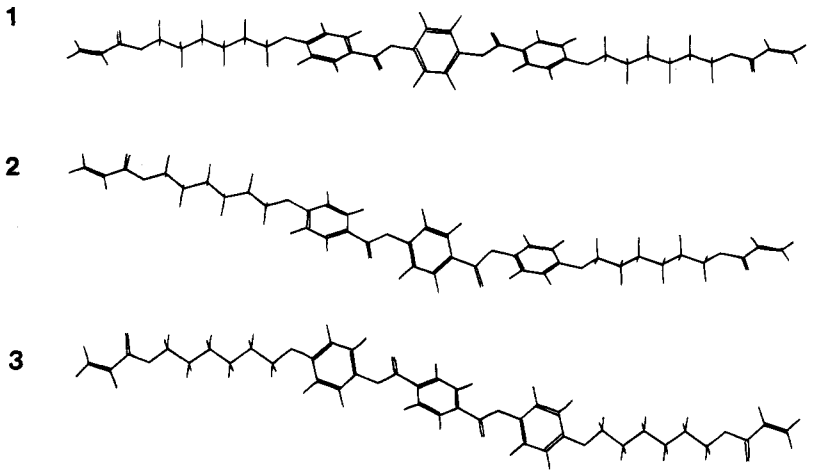

Figure 11. Minimum energy geometry of the monomers as calculated by AM1.

different behavior was observed. In the nematic phase, polymerization led to the formation of transparent networks. In the mixtures showing the S_a phase (no S_c phase), the order was disturbed on the microscopic scale, broke up into small layers, and became disoriented as in the case of pure 3. However, in the mixtures showing both the S_c and S_a phases the microscopic structure remained unaffected. We also performed experiments using the mixtures which showed both the S_a and S_c phases at lower temperatures. The mixture of monomer **1** and **3** (1:1) was polymerized at various temperatures within the smectic phases. The polymers were obtained in the S_a and S_c phases (at 105 and 80 °C, respectively). Polymerization at 70 °C resulted in a polymer film that was much clearer than those obtained in the other phases. A more careful inspection showed that the mixture entered a different phase prior to polymerization. X-ray diffraction revealed that this phase was the smectic-B phase (S_b). The X-ray diffraction photo of the polymer obtained in this phase is shown in Figure 6a. The sharp wide angle peaks observable in addition to the small angle diffraction peaks indicate that the molecules retained their well-defined microscopic order during polymerization. In Figure 6b we schematically summarize the changes taking place in the structure during polymerization in various phases for molecule **3** and its mixtures. Isomer **3** shows the same tendency to form a S_c phase as isomer **2** when mixed with **1**. However, monomer **3** and its mixtures with **1** in the S_a phase lost their microscopic structure upon polymeri-

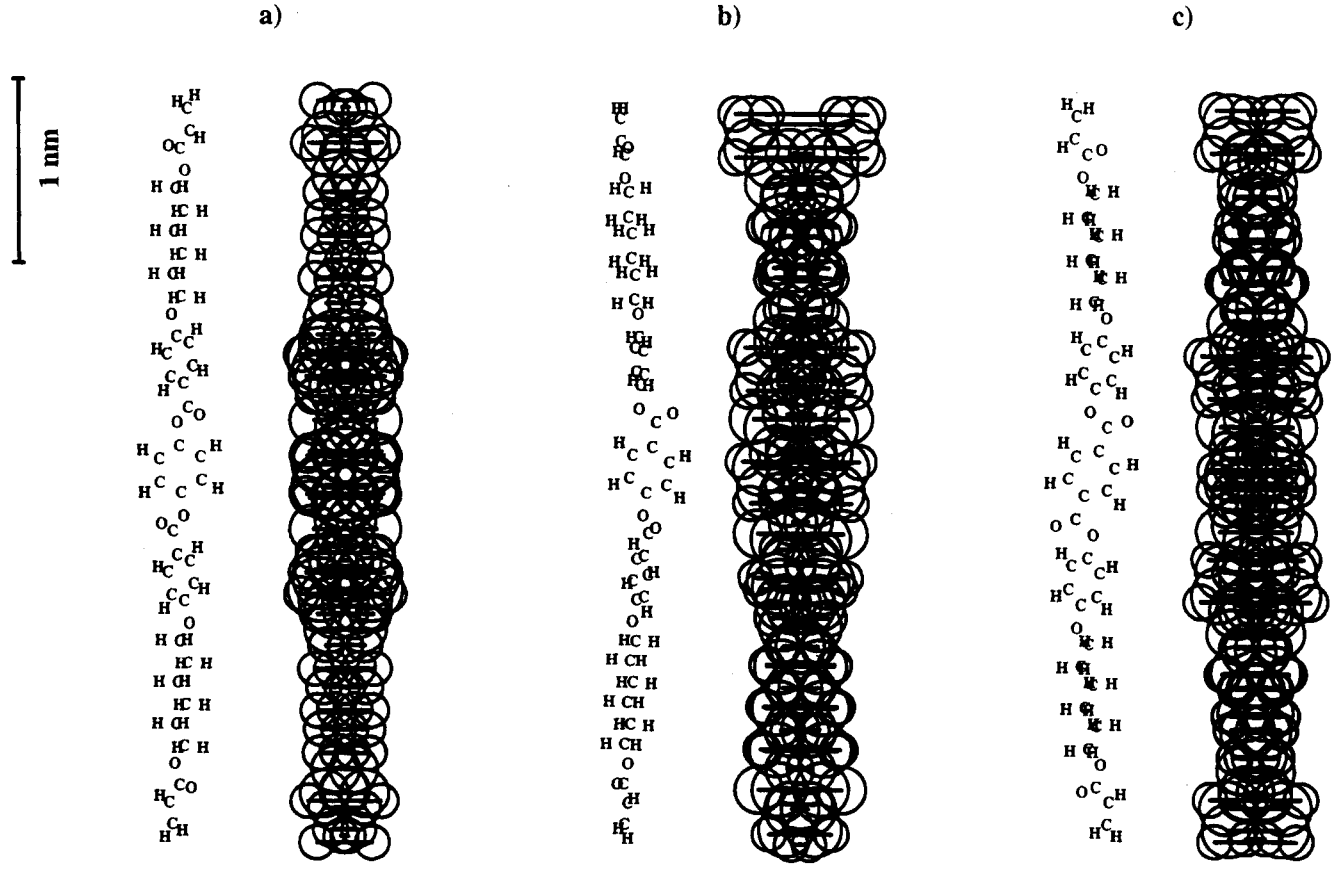

Figure 12. Rotational envelopes of the monomers obtained by rotation about the long axis: (a) **1**, (b) **2**, (c) **3**.

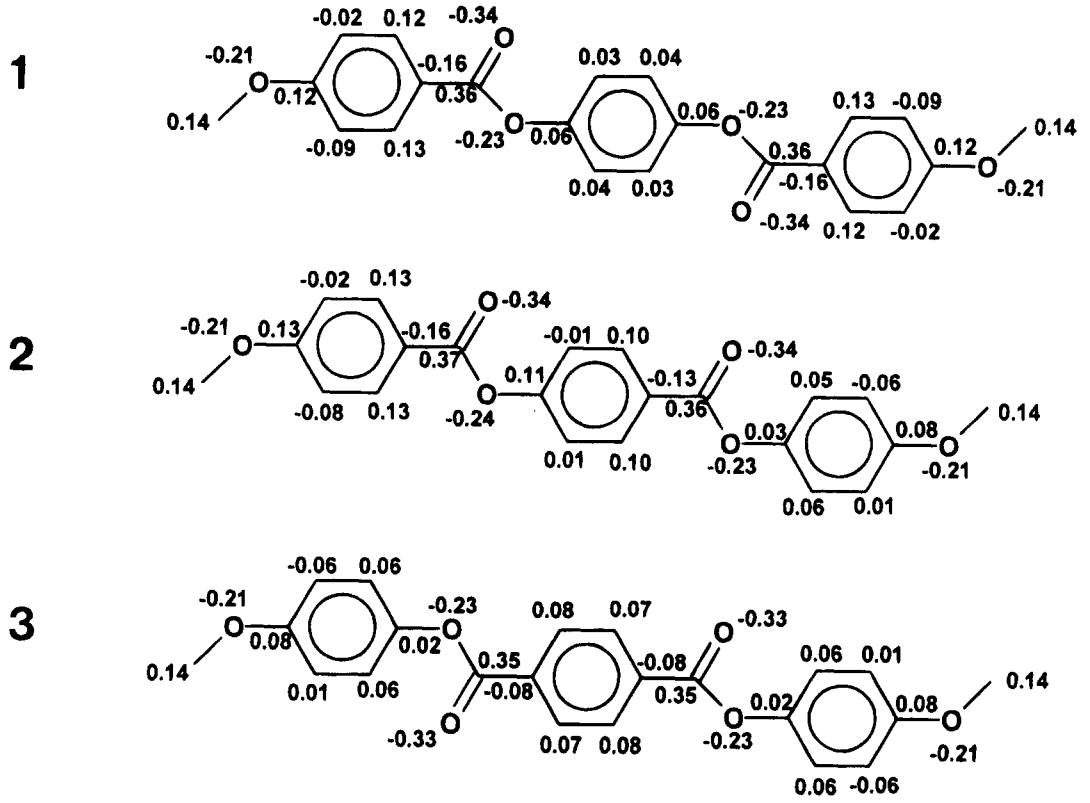

Figure 13. Mulliken charges obtained from the minimum energy electronic structure. For clarity only the central units are shown. The charge on carbon represents the charge on CH where appropriate.

Table 3. Rotational Barriers (kJ/mol) of C–O Bonds

molecule	C(H)OCC	CCC(=O)O	CC(=O)OC	C(=O)OCC
1	10.7	12.3	22.6	4.1
2	10.7, 4.1	12.3	22.6	4.1
3	4.1	10.3	22.6	4.1

zation whereas monomer **2** and its mixtures with **1** preserved their microscopic structure in the S_a phase. This indicates that the tendency to form the S_c phase is not the cause of the loss of microscopic structure as a result of polymerization observed for **3**. It also shows that successful polymerization, in which the microscopic structure is preserved is not dependent on the phase but the molecules. In the case of the S_c and S_b phases where the degree of order is higher, the fact that the microscopic structure of the mixtures (**3** and **1**) was preserved indicates that the strength of association between the molecules in these phases and their arrangement with respect to one another are responsible for the preservation of the macroscopic orientation during polymerization.

3.5. Ferroelectric Switching. It is well-known that systems showing the S_c phase can easily be doped using chiral molecules in order to produce a ferroelectric phase. In order to investigate the degree of association of the molecules we looked at the ferroelectric switching behavior of monomer **1** and of a mixture of monomer **1** with **3** (66% **1**). We provided these two systems with 1% chiral dopant. We then placed 2 μm thick cells containing the mixtures in the ferroelectric phase between crossed polarizers and measured the intensity of the light passing through the crossed polarizers during the application of a triangular voltage wave. The transmission voltage curves obtained for the mixture are shown in Figure 8. The mixture containing 66% **1** shows the behavior typical of a ferroelectric material. The transmission change between the dark and bright states as the molecules change the tilt direction during the switching, is schematically represented in Figure 9 (type 1). The changes in the orientation of the molecules could be followed under the optical microscope between the crossed polarizers as the cell had to be rotated for total extinction when the field was reversed. In the case of the system containing only **1**, however, a different behavior was observed during the switching: only flashes of increased intensity as shown in Figure 8 were observed. Under the microscope it was found that the molecules remained uniaxially oriented as the direction of the field was reversed. This behavior can be explained in terms of layer reorientation during switching, as schematically shown in Figure 9 (type 2). This is rather different from the behavior observed in the previous case. The different behavior of monomer **1** may also be due to the strong association between molecules **1** which decreases in strength within the mixtures.

3.6. Dielectric Permittivity. The dielectric permittivity gives information on the dipoles of the molecules and the degree of association between the molecules. We measured the dielectric permittivities of the molecules at 1 kHz in the LC state in the directions parallel ($\epsilon_{||}$) and perpendicular ($\epsilon_{\perp}$) to the director by changing the orientation of the molecules with respect to the electrodes. The results are shown in Figure 10. It can be seen that the dielectric anisotropy($\Delta\epsilon = \epsilon_{||} - \epsilon_{\perp}$) of molecules **1** and **3** is negative whereas that of molecule **2** is positive. Furthermore, the mean dielectric permittivity ($\langle\epsilon\rangle$) of molecule **2** is the highest whereas that of molecule **3** is lowest. For centrosymmetric molecules of **1** and **3** the net dipole would be expected to be 0, while isomer **2** would be expected to have a net dipole (see the section on molecular modeling). The

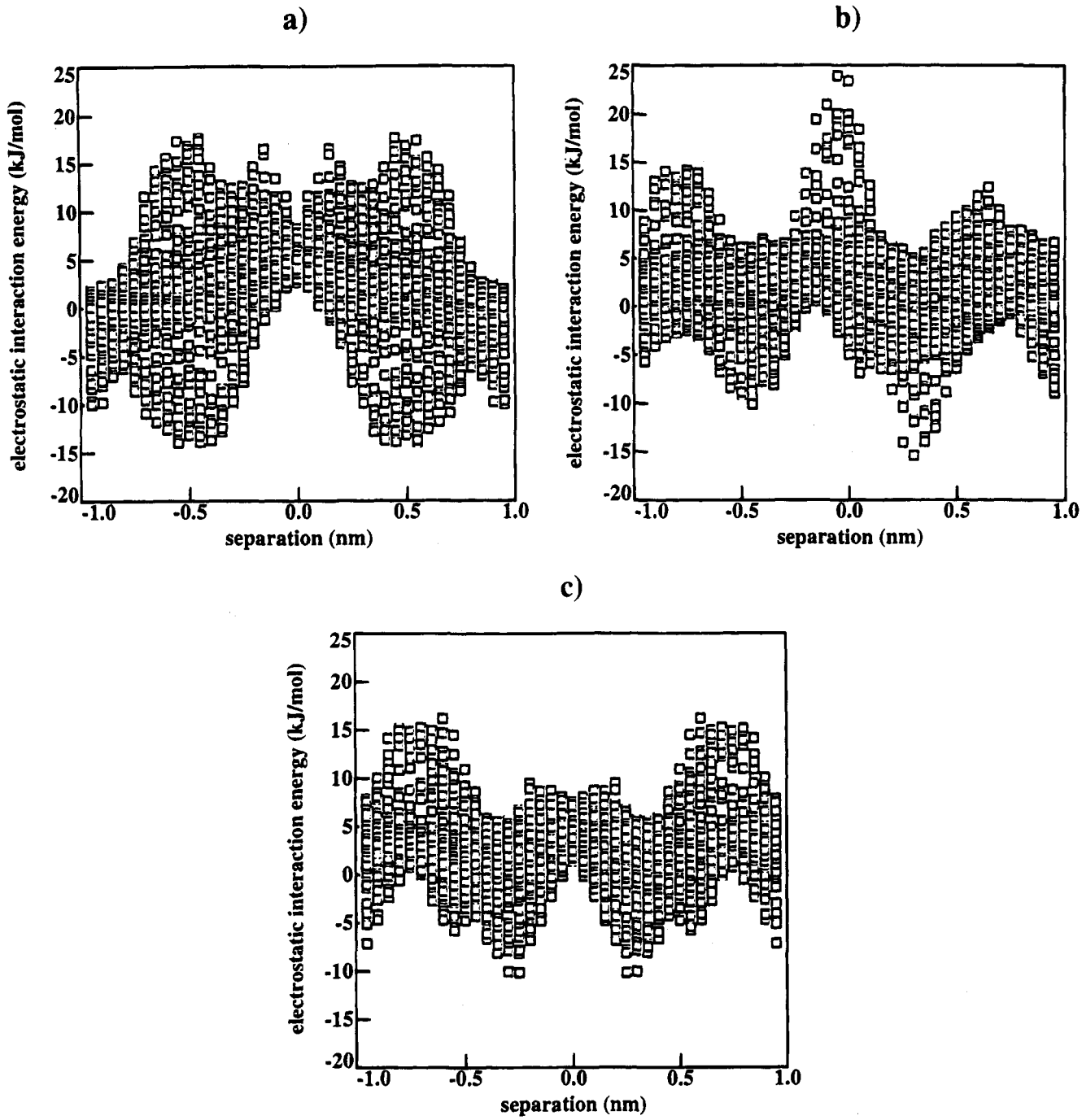

Figure 14. Electrostatic interaction energy of a dimers of various molecules obtained at the surface defined by the van der Waals contact: (a) **1**, (b) **2**, (c) **3**.

fact that the $\langle\epsilon\rangle$ of **2** differs only slightly from that of isomers **1** and **3** indicates a high degree of association in these systems.

3.7. Molecular Modeling. 3.7.1. Geometry. The minimum energy geometry of the molecules as calculated with the aid of the semi-empirical Hamiltonian AM1[15] (available in Mopac 6.0[16]) is shown in Figure 11. The geometry has inversion symmetry; the tails were positioned so as to obtain a conformation of maximum length. As expected, due to steric hindrance the molecules are not planar. Specifically, the torsion angle of the C—O bond next to the middle phenyl ring, C(=O)-OCC, is 51°. This value compares well with the 60° angle found in the crystal structure of 4-butylphenyl ((4'-butylbenzoyl)oxy)benzoate.[17] All the other torsion angles are within 30° of planarity. In the case of **1** with the exception of the central phenyl ring, all the atoms are more or less in the same plane. The geometry of the optimized structures of **2** and **3** show similar torsion angles. In the case of **2**, the C(=O)OCC angles are +53 and −45°, whereas that of **3** is 54°. Due to the different orientation of the ester bonds, the general shape is different from that of **1**. Compound **2** consists of three nonparallel planes, one end including an outer phenyl ring with a tail and an ester group, the other end just phenyl and the tail. The middle plane contains the central ring and an ester group. The middle plane of compound **3** consists of the central ring plus two ester groups, while the outer planes consist of a phenyl ring plus a tail. Another way to look at the space requirements of the molecules is to look at the structure obtained by rotation about the long axis. These rota-

tional envelopes are shown in Figure 12. The long axis is defined as the principal axis of inertia with the lowest moment. Although all the structures in the first instance look the same, there are some differences to be seen. Since **2** is not inversion symmetric, its rotational envelope is asymmetric. Clearly, **1** is smaller in width than **2** and **3**, the width being determined by the outer phenyl rings. To give an impression of the internal flexibility of the molecules the rotation barriers are given in Table 3.

It can be seen in Table 3 that the torsion angle which causes the structures to be nonplanar is also the one which has the lowest barrier: the barrier occurs at 0°. There is also an even lower barrier at 90°. Higher barriers are observed when an electron-donating oxygen is para to an electron-withdrawing carboxyl group. It is clear that the different patterns of the rotation barriers in the molecules causes a different internal motion upon thermal excitation. Most of the motion will occur in the rotational modes with the lowest barriers. This implies that in **1** the middle ring will move most easily whereas in **2** and **3** the outer rings will move most easily. As the outer phenyl rings determine the maximum width of the molecule upon rotation, the packing of **1** is more easily sustained with increasing temperature.

3.7.2. Refractive Index and Birefringence. The refractive index and intrinsic birefringence are related to the polarizability of a molecule by the Lorentz–Lorentz formula. The polarizability is easily computed if it is assumed to be the sum of bond polarizabilities. Following this procedure, the details of which are described elsewhere,[18] the refractive index at a density of 1.15 g/cm^3 is calculated to be 1.536. The intrinsic birefringence values of **1**–**3** are 0.199, 0.195, and 0.194, respectively. In accordance with the rotational envelopes of Figure 12, the intrinsic birefringence of **1** is highest followed by those of **2** and **3**, respectively.

3.7.3. Charge Distribution. The charges obtained in a Mulliken population analysis of the minimum energy electronic structure as calculated by AM1 are shown in Figure 13. For clarity, only the mesogenic group is shown and the charge on carbon represents the charge of the CH group where appropriate. The dipole moment of **2** is found to be 5.7 D, whereas the dipole moments of **1** and **3** are 0.0, because they are inversion symmetric. As expected, the largest charge separation is found on the ester groups. Due to the different orientation of the ester groups small differences in charge distribution occur on the phenyl groups. Most notably, however, the tail oxygen is seen to carry a negative charge which is the same in all compounds. Apparently, AM1 pays proper respect to the electronegativity of the oxygen atom. This does not imply that AM1 is ignorant of the push–pull effect characteristic of 1,4-substituted donor-acceptor benzenes. Indeed, the barrier heights of Table 3 show that this is not the case. This matter is of some importance since it has been argued[19] that the charge difference on the tail oxygen is responsible for the difference in phase behavior. The present calculations do not lend support to this argument.

3.7.4. Intermolecular Interaction of Dimers. To get some indication of the difference in favorable packings of the compounds under consideration and the importance of the charge distributions in the compounds, we will consider the electrostatic interaction energy of dimers. It is neither easy nor very useful to find the conformation of the lowest energy of such a dimer, since the potential energy surface has very many local minima of more or less the same energy. On the other hand, it is not easy to envisage the entire potential surface since it is a six-dimensional space. The results depicted in Figure 14 present an intermediate approach. Each marker corresponds to a situation in which the two molecules are just in van der Waals contact. All the points combined therefore represent a van der Waals surface obtained by translating one molecule with respect to the other. During these translations the relative orientation of the two local axes systems remains fixed. For each different relative orientation a different graph would be obtained. The graphs shown for compounds **1** and **3** correspond to the situation where the local axes are coincident. For compound **2** the axes systems are related by inversion symmetry. This guarantees that the ensemble will have no net dipole moment. The electrostatic interaction energy is calculated using the Mulliken charges of Figure 13. Mulliken charges are probably not the best set of charges to calculate the interaction energy, but they should allow a useful comparison among these related compounds.

Comparison of the graphs of Figure 14 shows that in all three cases the most favorable interaction is obtained when the molecules are shifted with respect to one another. This tendency is most apparent in the case of **1** and the least in the case of **2**. The molecules tendency toward a shifted arrangement with respect to one another can lead to the formation of a S_c phase. In terms of energy, the association of **2** seems to be the strongest. This can be understood from the fact that it has a net dipole moment. The interaction of **1** is however almost as strong, and this strong interaction is observed in many positions, which implies that it will stabilize the shifted conformation entropically. The interaction of **3**, however, is significantly weaker.

4. Conclusions

The syntheses of three isomeric LC diacrylates were described and their properties compared. The orientation of the ester bonds with respect to the central phenyl ring has a large effect on various properties of the isomers. All the isomers showed nematic phases. Isomers **2** and **3** showed S_a phases while isomer **1** showed a S_c phase. In the case of monomers **1** and **2** the order parameter of the networks increased with decreasing polymerization temperature. In the case of monomer **3** the opposite behavior was observed. Polymerization of molecules **1** and **2** in the smectic phases could be performed successfully and the microstructure was sustained. Monomer **3**, however, changed its appearance upon polymerization in the S_a phase. X-ray diffraction revealed that the smectic layers broke up and became disoriented upon polymerization. Dielectric measurements and ferroelectric switching indicated that monomers **1** and **2** showed association. This was also supported by the results of molecular modeling. The strength of association between the molecules is believed to be responsible for the preservation of the order within these systems upon polymerization rather than the phase.

References and Notes

(1) (1) Broer, D. J.; Gossink, R. G.; Hikmet, R. A. M. *Die Angew. Makromol. Chem.* **1990**, *183*, 45.

(2) Hikmet, R. A. M.; Lub, J.; Maassen van den Brink, P. *Macromolecules* **1992**, *25*, 4194.
(3) Broer, D. J.; Hikmet, R. A. M.; Challa, G. *Makromol. Chem.* **1989**, *190*, 3202.
(4) Hikmet, R. A. M.; Lub, J.; Higgins, J. A. *Polymer* **1993**, *34 (8)*,1735.
(5) Hikmet, R. A. M.; Howard, R. *Phys. Rev. E*,**1993**, *48*, 2752.
(6) Hikmet, R. A. M.; Zwerver, B. H. *Mol. Cryst. Liq. Cryst.* **1991**, *200*, 197.
(7) Hikmet, R. A. M.; Zwerver, B. H. *Liquid Cryst.* **1993**, *13*, 561.
(8) Kitzerow, H. S.; Schmidt, H.; Ranft, A.; Hepke, G.; Hikmet, R. A. M.; Lub, J. *Liq. Cryst.* **1993**, *14*, 911.
(9) Hikmet, R. A. M. *Macromolecules* **1992**, *25*, 5759.
(10) Broer, D. J.; Boven, J.; Mol, G. N.; Challa, G. *Makromol. Chem.* **1989**, *190*, 2255.
(11) Jahromi, S.; Lub, J.; Mol, G. N. *Polymer* **1994**, *34*, 622.
(12) Lub, J.; Broer, D. J.; Hikmet, R. A. M.; Nierop, K. G. J. *Liq. Cryst.*, in press.
(13) Takenaka, S.; Sakurai, Y.; Takeda, H.; Ikemoto, T.; Miyake, H.; Kusabayashi, S.; Takagi, T. *Mol. Cryst. Liq. Cryst.* **1990**, *178*, 103.
(14) De Vries, A. *Mol. Cryst. Liq. Cryst.* **1985**, *131*, 125.
(15) Dewar, M. J. S.; Zoebisch, E. G.; Healy, E. F.; Stewart, J. J. P. *J. Am. Chem. Soc.* **1985**, *107*, 3902.
(16) Stewart, J. J. P. MOPAC (V6.0): A general orbital package. QCPE 455; Quantum Chemistry Program Exchange, Indiana University: Bloomington, IN, 1985.
(17) Birner, P.; Kugler, S.; Simon, K.; Naray-Szabo, G. *Mol. Cryst. Liq. Cryst.* **1982**, *80*, 11.
(18) Aerle, N. A. J.; Tol, A. J. W. *Macromolecules*, **1994**, *27*, 6520.
(19) Goodby, J. W. In *Ferroelectric Liquid Crystals*; Taylor, G. W., Ed.; Gordon and Breach: Reading, MA, 1991; Vol. 7, p 174.

MA9460504